PCCP

Volume 1 | Number 1 | Jan 2013 | Pages 1–100

PCCP

Physical Chemistry Chemical Physics
www.rsc.org/pccp

ROYAL SOCIETY OF CHEMISTRY

ROYAL SOCIETY OF CHEMISTRY

www.rsc.org/pccp

One sentence abstract:

Fat containing and defatted human serum albumin adsorption to silica nanoparticles have different structures and time dependence to form.

Human Serum Albumin Binding to Silica nanoparticles
- effect of protein fatty acid ligand

Joo Chuan Ang[a], Mark J. Henderson[a], Richard A. Campbell[d], Jhih-Min Lin,[a] Peter N. Yaron,[a] Andrew Nelson[c], Thomas Faunce[b] and John W. White*[a]

[a] Research School of Chemistry and [b] College of Law, Australian National University, ACT 0200, Australia
[c] Australian Nuclear Science and Technology Organisation, Sydney, Australia
[d] Institut Laue-Langevin, Grenoble, France.[§]

[*]Corresponding author. Email: jww@rsc.anu.edu.au

Neutron reflectivity shows that fatted (F-HSA) and defatted (DF-HSA) versions of human serum albumin behave differently in their interaction with silica nanoparticles premixed in buffer solutions although these proteins have close to the same surface excess when the silica is absent. In both cases a silica containing film is quickly established at the air-water interface. This film is stable for F-HSA at all relative protein/silica concentrations measured. This behaviour has been verified for two small silica nanoparticle radii (42Å and 48Å). Contrast variation and co-refinement have been used to find the film composition for the F-HSA–silica system. The film structure changes with protein concentration only for the DF-HSA–silica system. The different behaviour of the two proteins is interpreted as a combination of three factors: increased structural stability of F-HSA induced by the fatty acid ligand, differences in the electrostatic interactions, and the higher propensity of defatted albumin to self-aggregate. The interfacial structures of the proteins alone in buffer are also reported and discussed.

1   Introduction

This paper compares the air-water interface structure of native "fatted" and "defatted" human serum albumins, F-HSA and DF-has when mixed with silica nanoparticles at pH ca 7. This work relates to the known nanotoxicology of silica[1,2,3] through interactions with proteins The air-water interfacial structure is a sensitive means of detecting these interaction[4] and isotopic contrast variation in neutron reflectivity[5] has proven effective in finding quantitative information about the

protein/nanoparticle composition at the interface.

Human serum albumin (HSA), a 66.5 kDa molecule with 585 amino acid residues, is chosen as the most abundant protein in human blood plasma (~40 mg/mL). . The solution structure of "native" (fatted) HSA is known as approximately heart-shaped[6] with 80 Å edges and 30 Å thick. The HSA structure is stabilized by 17 disulfide bonds located throughout the protein sequence, with a lone cysteine residue near the N-terminus (Cys_{34}), which stabilizes the protein against thermal denaturation[7] up to 60ºC. Given its structural flexibility to accommodate so many different lipophilic molecules, it is therefore not surprising that HSA is also able to bind a wide variety of drugs[8] such as aspirin, warfarin and ibuprofen. The molecular properties, X-ray and neutron scattering length densities (SLD_x and SLD_N) of the proteins are given in Table 1.

Table 1 Properties of F-HSA, DF-HSA and Ludox® SM-30 silica nanoparticles.

	F-HSA	DF-HSA	LS-30 (r = 42 Å)	SM-30 (r = 48 Å)
Molecular volume ($Å^3$)	88249^8	99249^a	3.1×10^5	4.6×10^5
Estimated α-helix %	71^{10}	67^9	n/a^9	n/a^9
Isoelectric point	4.7^{11}	5.8^{12}	>2	> 2
Net charge at pH 7	-17^a	-15	+9	+9
$SLD_x /Å^{-2}$	11.7×10^{-6}	12.1×10^{-6}	18.9×10^{-6}	18.9×10^{-6}
$SLD_N/Å^{-2}$	1.58×10^{-6}	1.66×10^{-6}	3.47×10^{-6}	3.47×10^{-6}

[a] Assuming two fatty acids (FA) bound per F-HSA.

A total of seven binding sites for long-chain FA (C16:0-palmitic acid and C18:0-stearic acid) were reported by Curry and co-workers[8]. Of these, there are three high-affinity binding sites for palmitic acid[13]. Under normal physiological conditions, HSA carries an average of 2 molecules of FA per protein molecule but the molar ratio of fatty acids can increase to 6 or greater during fasting or extreme exercise or under pathological conditions such as diabetes and liver disease. In our present work, we assume that the fatted HSA has 2 molecules of FA per HSA. Other important properties of the molecules have been reviewed by Curry[14].

Our choice of the closely similar F-HSA and DF-HSA molecules to probe silica binding exploits this similarity and their differences seen by Leggio et al. They follow different denaturation pathways in the presence of denaturants[15] attributable to the fatty acid ligand (palmitic acid) of FHSA conferring resistance to urea denaturation[6].. The goal is to understand at high resolution and in buffer, the bulk and interfacial properties of small "engineered" nanoparticle - complexes relevant to nanotoxicology. Already we have explored the silica/β-casein system, where the robustness of the surface film to dissolution dilution was strong[4], and the non-equilibrium aspects of kinetically-trapped protein films.

2   Experimental Details

2.1   Materials

Lyophilized F-HSA (A8763) and DF-HSA (A3782), both with purity greater than 99%, were purchased from Sigma-Aldrich. Both were used as received without any further purification. Two forms of silica, Ludox® SM-30 and LS-30, were procured from Sigma-Aldrich, and purified light water (Milli-Q 18.2 MΩ·cm) used for all sample preparation. Deuterated water (99.9%) from Sigma was used for neutron reflectivity experiments. For nanotoxicological comparisons, the nature of the silica was characterized by small angle x-ray scattering at the Australia Synchrotron and the European Synchrotron Radiation Facility (ESRF, Grenoble). Particle radii of 48 Å and 42 Å respectively were found in good agreement with the manufacturer's quoted surface area. Further information about the two nanoparticle samples may be found in Table 1 and Figure SI1 shows the small angle x-ray scattering from the three particles bein used in these studies. The HSA stock solutions were prepared in phosphate buffer and kept below 4°C to minimize protein aggregation until use.

2.2   Sample preparation

All samples were made in standard phosphate buffer solution (PBS; 50 mM, pH 6.9). Preliminary experiments were performed on HSA-silica solutions (Ludox® LS-30 and/or SM-30) using x-ray reflectivity at the Research School of Chemistry (ANU), and on solutions of Ludox® LS-30 on the PLATYPUS neutron reflectometer (ANSTO) and Ludox® SM-30 on the FIGARO neutron reflectometer ILL (Grenoble) The F-HSA and DF-HSA concentrations used for neutron reflectivity measurements at PLATYPUS were between 0.01, 0.1, 1.0 and 2.0 mg/mL. Ludox® LS-30 nanoparticle suspension was premixed with the protein in PBS to bring the silica nanoparticle concentration in solution to 0.6% v/v (silica). The protein solution (0.1 mg/mL) was

prepared in Air Contrast Matched Water (ACMW) (8.1% D_2O and 91.9% H_2O by volume) in PBS. The stability of both fatted and defatted HSA solutions in standard phosphate buffer was studied with dynamic light scattering as a function of storage time and temperature. The protein radii were both ca 3.5nm as expected for monomers and the solutions stable beyond the time scale of the experiments (Supplementary Information Figure SI2). For the contrast variation measurements at FIGARO protein concentrations of 0.003 to 1.0 mg/mL of F-HSA only were premixed with diluted Ludox® SM-30 to reach 0.6% v/v (silica) in PBS. Here the subphase was either ACMW or D_2O. The mixing was done by pouring together equal volumes of protein and silica solutions at double their intended final concentrations immediately prior to the start of the measurements and the surface lightly aspirated to remove any kinetically trapped film.

2.3   X-ray and neutron reflectivity

Specular X-ray reflectivity was performed using an in-house angle-dispersive X-ray reflectometer at the Australian National University described elsewhere[16]. Measurements were made for $0.01 < Q/Å^{-1} < 0.45$. Neutron reflectivity measurements were performed on the time-of-flight neutron reflectometers PLATYPUS[17] (Bragg Institute, ANSTO, Australia) and at FIGARO (Institut Laue-Langevin, Grenoble, France)[18]. Neutron pulses were generated using a disk chopper system in high intensity mode ($\Delta\lambda/\lambda = 10\%$). Reflected neutrons were then recorded using a two-dimensional He^3 detector. Measurements were performed at Q_z-values from 0.01 to 0.4 $Å^{-1}$. Q_z is the wavevector momentum transfer in the direction perpendicular to the probed surface and is given by

$$Q_z = \left(4\pi/\lambda\right)\sin\theta \tag{1}$$

where λ is the X-ray wavelength (Cu k_α, 1.54 Å) and θ is the angle of incidence to the surface. The reflection of X-rays from an ideal interface, known as Fresnel reflection, decays to the 4th power in Q_z and is given by

$$R_F \approx \left(Q_c/2Q_z\right)^4 \tag{2}$$

where Q_c is the critical angle for total external reflection. Hence, all X-ray and neutron reflectivity profiles shown will be Fresnel-corrected, RQ_z^4 versus Q_z, to highlight the differences from an ideal vacuum/material interface reflection.

The samples were prepared immediately prior to the measurement and measured in temperature-controlled (20 °C) sealed troughs to limit evaporation. MOTOFIT[18] was used in the X-ray and neutron reflectivity data fitting process.

The surface excesses of protein (Γ_P) and silica nanoparticle (Γ_S) adsorbed at the air-water interface can be extracted from measurement of protein-nanoparticle solutions under the ACMW condition, where the scattering length density of bulk water is zero, namely

$$\Gamma = \Phi \cdot \tau \cdot \rho' \tag{3}$$

$$\Phi = {}^{\rho}/_{\rho_P} \tag{4}$$

where Φ is the volume fraction, τ is the layer thickness, ρ' is the physical density, ρ and ρ_P are the measured and theoretical scattering length densities of the protein respectively. By analogy with the structure of β-casein/silica nanoparticle[4] where the silica was sandwiched by protein in the vertical direction, we assume that Γ_S can be calculated by substituting for the relevant parameters in the silica nanoparticle layer. The number of protein molecules (N_P) and silica nanoparticles (N_S) adsorbed within the interfacial layer for the same area is then given by

$$N_P = {}^{\Gamma_P \cdot N_A}/_{MW} \tag{5}$$

$$N_S = {}^{\Gamma_S}/_{M_S} \tag{6}$$

The protein to nanoparticle ratio for a given area is then straightforward.

$$\Psi = {}^{N_P}/_{N_S} \tag{7}$$

3   Results

3.1   Structure of HSA at the air-water interface

As a preliminary to the concentration dependent silicate mixture measurements, the structure of both HSA molecules at the air-water interface of standard phosphate buffer was studied as a function of protein concentration by a combination of X-ray and neutron reflectivity.

3.2   X-ray Reflectivity

Figure 1 (A) and (B) shows the x-ray reflectivity (XRR) multiplied by Q^4 for pre-mixed solutions of F-HSA and DF-HSA (respectively). The high Q part of the data shows an increase in roughness with concentration (Table 2). Figure 2 (A), (B) show the corresponding real space profiles obtained by constrained fitting with MOTOFIT[19]. The differences in these profiles and the electron density profiles (Figure 2) were the first indication of subtly different surfactancies for the two proteins.

(A)   **(B)**
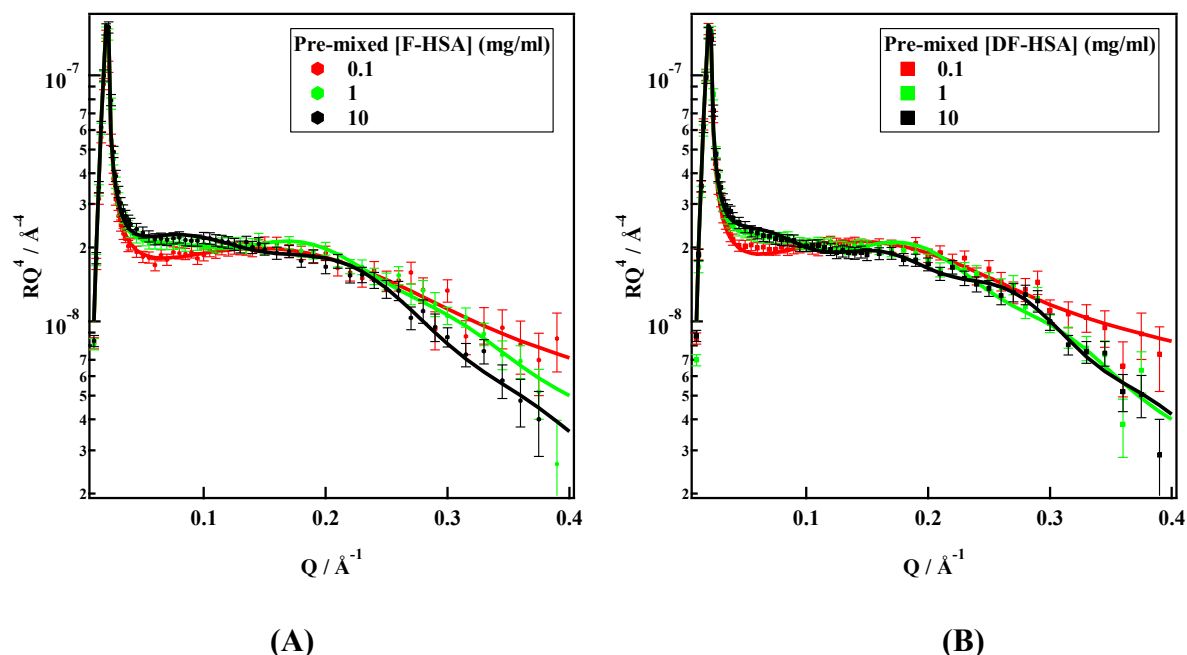
Fig. 1 **X-ray reflectivity profiles for pre-mixed F-HSA (A) and DF-HSA (B) layers at the air-water interface for 0.1 (red), 1 (green) and 10 (black) mg/mL in PBS at 25 °C.**

5

The fitting parameters from XRR data of HSA layers at the air-water interface are shown in Table 2 where the thicknesses of layers 1, 2 and 3 descending from the surface are τ_1 τ_2 τ_3 and ρ_1 ρ_2 ρ_3 their scattering length densities and roughness σ_1 σ_2 σ_3. The scattering length density profiles are shown in Figure 2.

A   B
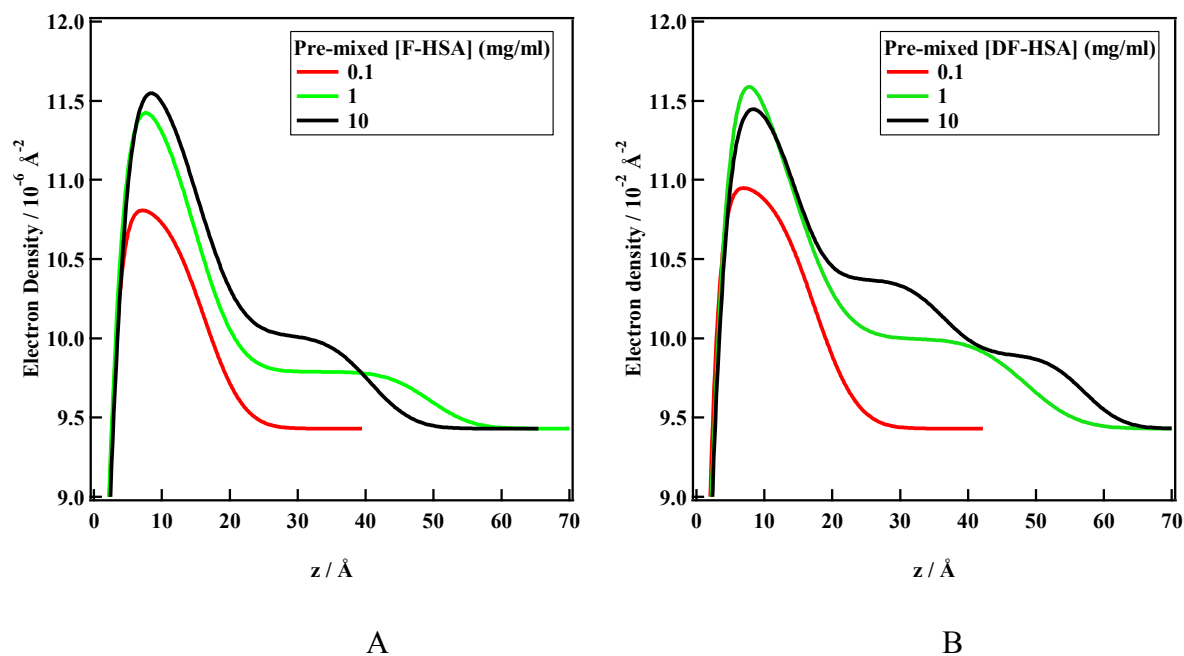
10

Fig. 2 **X-ray electron density profiles for pre-mixed F-HSA (A) and DF-HSA (B) layers at the air-water interface for 0.1 (red), 1 (green) and 10 (black) mg/mL in PBS at 25 °C.**

Table 2. Fitting parameters from XRR data of HSA layers at the air-water interface.

mg/mL HSA	F-HSA			DF-HSA		
	0.1	1	10	0.1	1	10
τ_1 / Å	16 (2)	15 (1)	15 (1)	17 (1)	15 (1)	14 (1)
$\rho_1/10^{-6}$Å^{-2}	10.8 (0.2)	11.6 (0.1)	11.8 (0.1)	11.0 (0.2)	11.8 (0.1)	11.5 (0.1)
σ_1 / Å,	2.4	2.9	3.4	2.2	3.0	3.1
τ_2 / Å		35 (2)	25 (1)		34 (1)	22 (2)
$\rho_2/10^{-6}$Å^{-2}		9.8 (0.1)	10.1 (0.1)		10.0 (0.1)	10.4 (0.1)
σ_2 / Å		5.0	5.0		6.0	3.8
τ_3 / Å						21 (1)
ρ_3 / 10^{-6} Å^{-2}						9.9 (0.1)
σ_3 / Å						4.5
Γ/mg·m^{-2}	1.2 (0.1)	2.4 (0.1)	2.9 (0.1)	1.5 (0.2)	2.9 (0.1)	3.3 (0.2)

5 Here τ_i / Å, $\rho_i/10^{-6}$Å^{-2}, σ_i / Å are the *i*th layer thickness, scattering length density and interfacial roughness respectively.

For both forms at the lowest HSA concentration of 0.1 mg/mL, the adsorbed interfacial protein has a 16 Å thick layer. A more diffuse second layer extending out to ca. 50 Å is observed when the protein concentration is above 1 mg/mL. At 10 mg/mL, the highest concentration measured, a third layer was necessary to fit the DF-HSA XRR data satisfactorily. This is a second indicator of different 10 surfactancy from F-HSA. The roughness for both proteins indicates multilayers formed at the air-water interface.

This interfacial dimension at 0.1 mg/mL is much thinner than expected from the protein native structure in solution at pH 7 found by small angle scattering[15]. This structure is closer to the heart-shaped structure observed by x-ray crystallography[9]. Our XRR results suggest that the sparse film of 15 F-HSA adopts a "train-and-loop"[20] structure at the air-water interface. The 16 Å thickness corresponds to the diameter of an α-helix barrel[21] and in this model, the α-helices would form the highly packed

"train" and the diffuse 35 Å layer below consist of "loops" of connecting segments between α-helices which protrude into the bulk subphase. This model is discussed more fully below.

3.3 Neutron reflectivity

3.3.1 low concentration solutions.

The neutron reflectivity profiles for 0.1 mg/mL F-HSA and DF-HSA in ACMW are shown in Figure 3 (a) and the corresponding scattering length density (SLD) profiles in Figure 3 (b). The best fit was again a 17 Å adsorbed protein layer at the air-water interface. The parameters (Table 3) show that a slightly thicker protein film resulted from DF-HSA with the same solution concentration and the thickness reduces with time- possibly because of protein loss from the surface to the subphase.
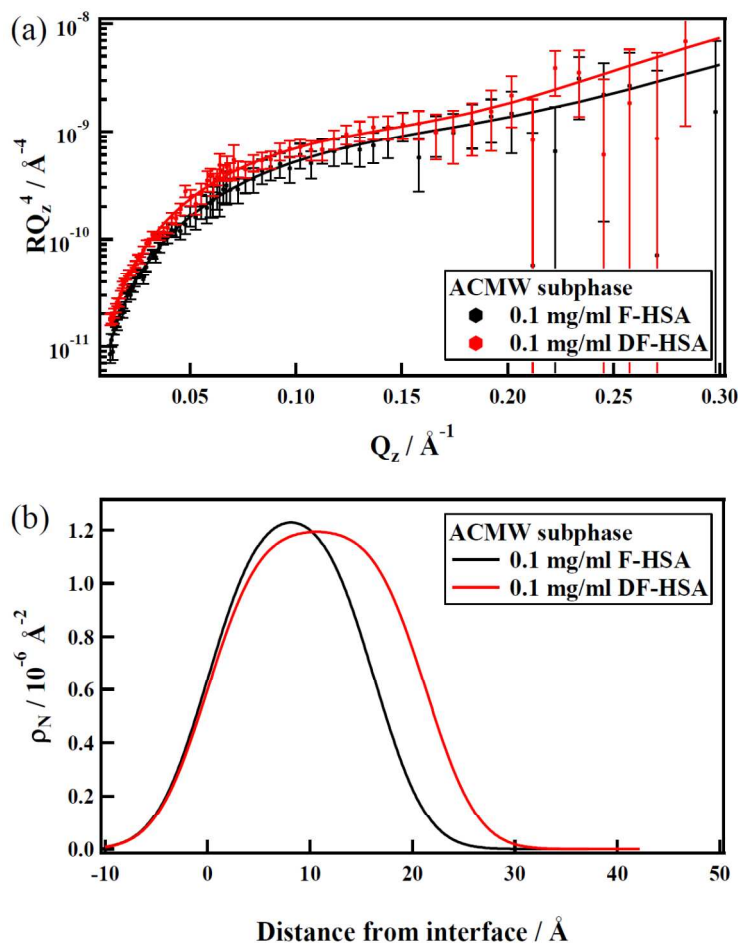
Fig. 3 (a) Semi-log plot of reflectivity profile (solid lines are fits to the data). (b) Real-space profile of the protein structure at the air-water interface. F-HSA and DF-HSA are shown in black and red respectively.

Table 3 ACMW sub-phase fitting parameters for 0.1 mg/mL fatted and defatted HSA.

Time / h	F-HSA			DF-HSA		
	τ / Å	ρ / 10^{-6} Å^{-2}	Γ / mg·m^{-2}	τ / Å	ρ / 10^{-6} Å^{-2}	Γ / mg·m^{-2}
1	17	1.07	1.3	26	0.90	1.6
10	17	1.28	1.5	21	1.20	1.8

3.3.2 Higher Protein Concentrations

For higher protein concentrations, the equilibrium (20 hours) X-ray reflectivity and electron density profiles for F-HSA are shown in Figures 4(a) and 4(b) respectively. A broader total layer is formed for 1 and 10 mg/mL solutions (Figure 4) consistent with published results[22].
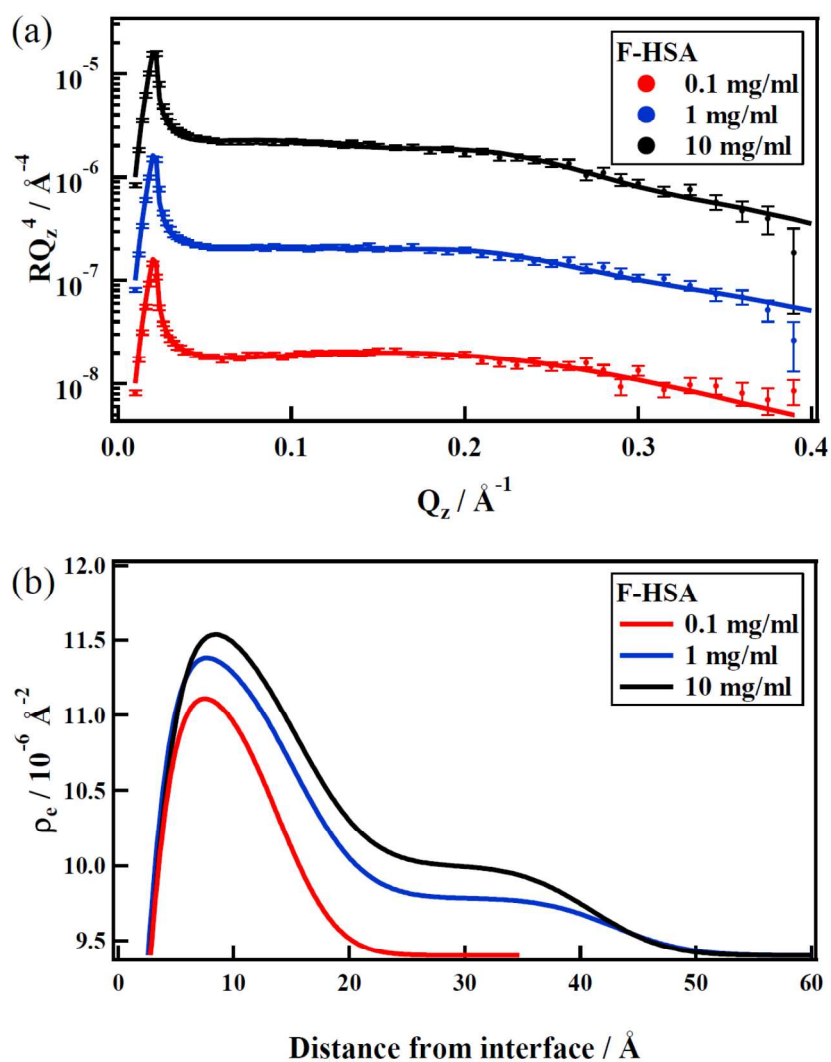
Fig. 4 (a) RQ^4 plots of the neutron reflectivity of F-HSA solutions (solid lines are fits to the data). Profiles are vertically offset for clarity. (b) Electron density profile of F-HSA at the air-water interface. 0.1 mg/mL (━), 1 mg/mL (━) and 10 mg/mL (━).

Table 4 X-ray reflectivity fitting parameters for 0.1, 1 and 10 mg/mL F-HSA solutions.

F-HSA concentration (mg/mL)	0.1	1	10
τ_1 / Å	14	15	15
ρ_1 / 10^{-6} Å^{-2}	11.3	11.5	11.7
τ_2 / Å	-	28	26
ρ_2 / 10^{-6} Å^{-2}	-	9.78	10.0
χ^2	2.2	1.7	1.9
Γ / mg·m^{-2}	1.3	2.2	2.6

3.4   X-ray reflectivity from F-HSA/SiO$_2$ mixtures

3.4.1   Effect of solution pH.

An experiment over the pH range 2.1 to 12.3 allowed the pH sensitivity of HSA adsorption onto SM-30 silica nanoparticles to be estimated. The same sol's interaction with β-casein[4] was previously shown to have a strong electrostatic component and, judging by the isoelectric points of both components here (Table 1), the interaction between the same silica and HSA should be similar. This was explored by systematically changing the sub-phase solution pH.

The data of Figure 5 show this to be so. There is strong adsorption of the silica from pH 2.1 to pH 7.2 though protein is also present in a near-surface monolayer at pH 2.1. No adsorption of the nanoparticles occurs at pH 12.3 for electrostatic reasons. The surface structure of the protein-nanoparticle complex observed at pH 2.1 has a more complete layer of protein (than at higher pH) with attached silica nanoparticle deeper into the interface.
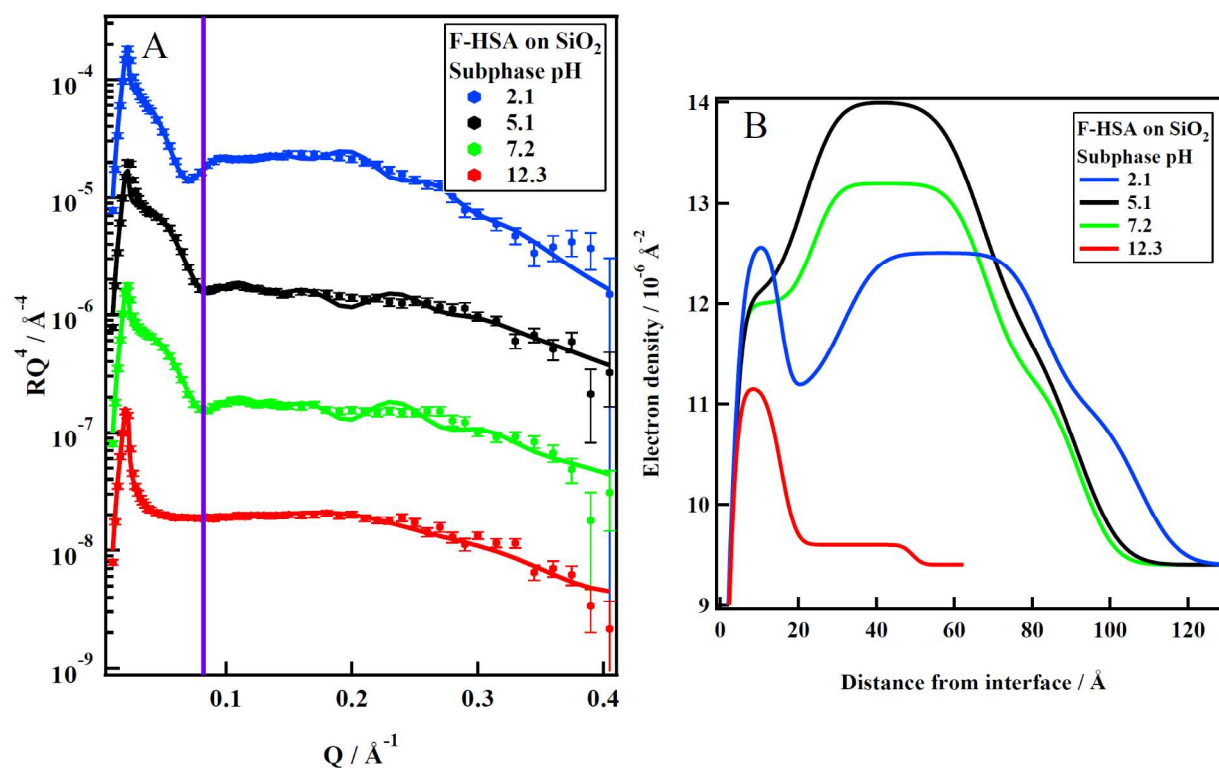
Fig. 5 (A) Equilibrium X-ray reflectivity of 0.5mg of F-HSA surface structures after interaction with SiO$_2$ nanoparticles at various pH values. (B) Electron density profiles for solution subphase pH of 2.1, 5.1, 7.2, and 12.3.
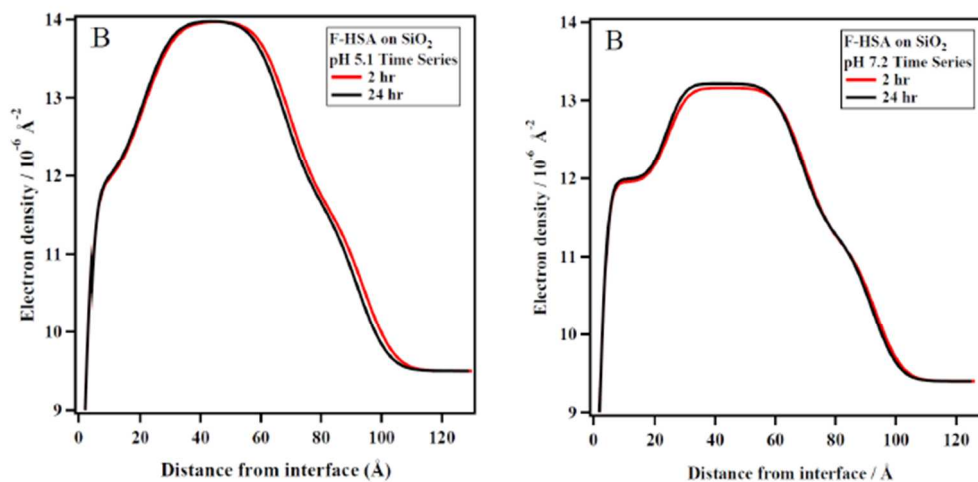
Fig. 6 Real-space electron density profiles of F-HSA-SiO$_2$ films on pH 5.1 and 7.2 subphase silica nanoparticle solution at 2 hours (red) and 24 hours (black).

Figure 6 shows that at pH 5.1 and pH 7.2 there is rapid equilibration of the surface protein-nanoparticle structure and no significant change in the profiles between 2 hours and 24 hours. At the neutral pH of 7.2, the equilibrium surface structure was achieved within 2 hours and the real space profile is very similar to that at pH 5.1. We note that the scattering length densities of the protein parts

and silica parts of the film are about 75% of those expected for the two dry constituents: protein (ca. 12 x 10^{-6} Å^{-2}) and silica (ca. 18.9 x 10^{-6} Å^{-2}), demonstrating the high coverage and close packing.

An important difference between F-HSA and DF-HSA is the value of the electron densities in each layer – the structure at pH 7.2 has significantly lower electron density in all the layers, most obviously the middle layer where most of the volume fraction is occupied by silica nanoparticles. This is consistent with the charge on the silica being smaller than that at pH 5.1 in accordance with the positions of the isoelectric points. The similar electron density values of the top layer for both surface structures at pH 5.1 and pH 7.2 indicate that this layer is mostly protein, with a small contribution from the silica. We conclude that rather less silica is attached to F-HSA at the air-water interface at pH 7.2 than at pH of 5.1. These data are a helpful clue to the layer compositions.

3.5   Neutron reflectivity of HSA/SiO$_2$ mixtures

Measurements were carried out on the HSA/LS-30 system (42-Å radius nanoparticles) at the PLATYPUS reflectometer using a subphase of buffered ACMW. Figures 7(a) and 7(b) show the neutron reflectivity profiles for increasing concentrations of F-HSA and DF-HSA respectively with a nanoparticle sol concentration of 0.6% v/v. The well-defined Kiessig fringe in the low-Q region (at ca. 0.04 Å^{-1}) appears in all data and indicates a structure of dimension ca. 150 Å. The different interactions of F-HSA and DF-HSA with SiO$_2$ nanoparticles are clear also. While the reflectivity signal as a function of concentration was constant and independent of the reaction time for F-HSA, that for DF-HSA first increased with higher protein concentration and then decreased as shown in Figure 7. Clearly competitive processes are occurring in forming the film for this protein.
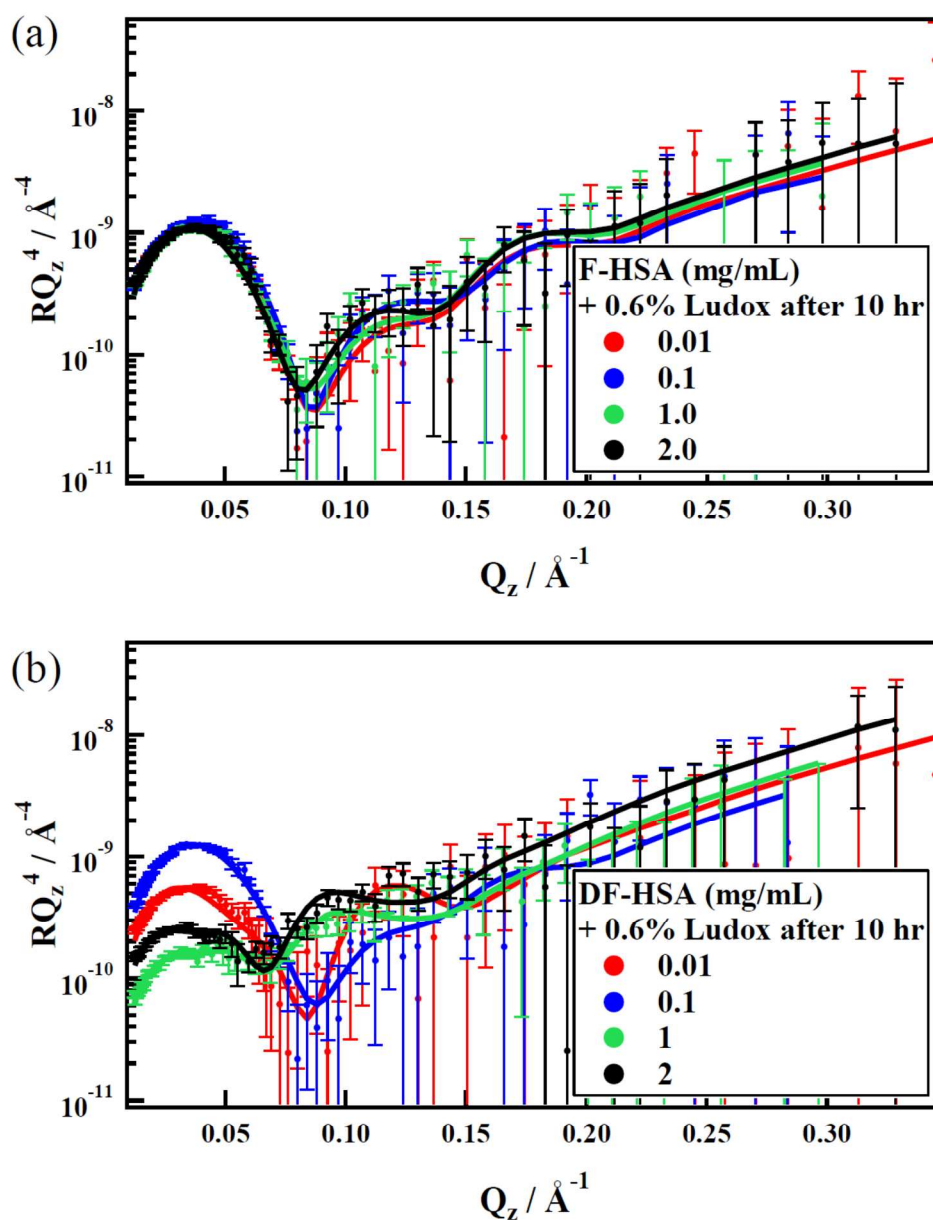
Fig. 7 Neutron reflectivity profiles of protein-nanoparticle mixtures as a function of protein concentration (a) F-HSA and (b) DF-HSA. The LS-30 nanoparticles were used and the data were recorded on PLATYPUS. Solid lines 5 are fits to the reflectivity data (fitting parameters for F-HSA and DF-HSA are shown in Tables 4 and 5 respectively).

The data for F-HSA are well fitted for all concentrations by a three layer model where scattering length densities and thickness are almost constant - as shown in Table 5.

Table 5 Neutron reflectivity fitting parameters corresponding to F-HSA with LS-30.

F-HSA:SiO$_2$ ratio	1:200	1:20	1:2	1:1
τ_1 / Å	27	24	29	29
ρ_1 / 10^{-6} Å^{-2}	0.68	0.70	0.67	0.78
τ_2 / Å	59	60	57	57
ρ_2 / 10^{-6} Å^{-2}	1.5	1.6	1.5	1.5
τ_3 / Å	34	32	35	35
ρ_3 / 10^{-6} Å^{-2}	0.33	0.30	0.35	0.29
χ^2	2.5	1.8	2.3	2.3

This is not true for DF-HSA where the fitting parameters vary with protein concentration (Table 6) as do the scattering length density distributions (Figure 8).

5

Table 6 Neutron reflectivity fitting parameters corresponding to DF-HSA with LS-30.

DF-HSA:SiO$_2$ ratio	1:200	1:20	1:2	1:1
τ_1 / Å	78	26	29	36
ρ_1 / 10^{-6} Å^{-2}	1.1	0.71	0.96	1.0
τ_2 / Å	54	59	59	58
ρ_2 / 10^{-6} Å^{-2}	0.26	1.6	0.39	0.59
τ_3 / Å	-	40	83	81
ρ_3 / 10^{-6} Å^{-2}	-	0.25	0.070	0.14
χ^2	1.9	1.5	1.0	1.4

The real space fitted scattering length distribution functions (Figure 8) show that for F-HSA, the interfacial structure extends to approximately 125 Å beneath the surface with low scattering length density protein above and below a silica-rich middle layer. For DF-HSA at the higher concentrations (1 and 2 mg/mL DF-HSA), the structure is quite different and the density distribution extends out to ca. 180 Å at the highest protein concentration.
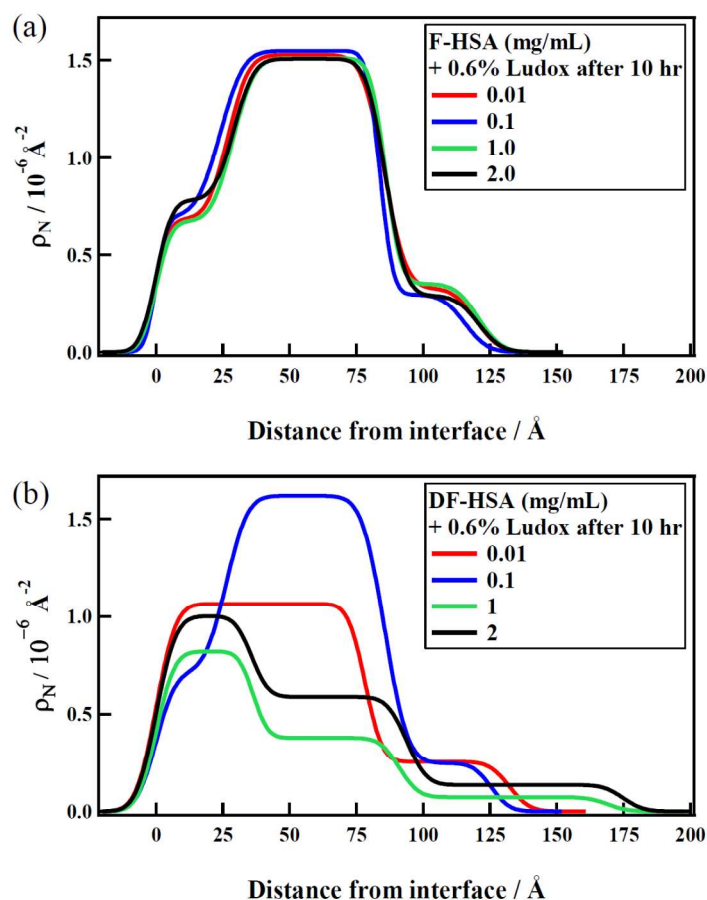
Fig. 8 **Real-space neutron scattering length density profiles corresponding to (a) F-HSA and (b) DF-HSA for four concentrations of protein relative to the constant 0.6%v/v LS-30 silica nanoparticles.**

For comparison with the x-ray result we recall the neutron scattering length densities of the components in Å^{-2}: F-HSA (1.58×10^{-6}); DF-HSA (1.66×10^{-6}); SiO$_2$ (3.47×10^{-6}). Here the layer 2 SLDs for the F-HSA system, for example, are only about 40% of the Silica SLD. The situation is similar for the protein component showing both the extra contrast in X-rays for both protein and silica, from the low scattering length density of water as well as the degree of ACMW mixing into the layer structures. Notable once again is the strong drop in SLD for the second layer in DF-the HSA/silica data.

3.6   Co-refined contrast variation of neutron reflectivity F-HSA/SiO$_2$ mixtures

Because of the concentration independence of the reflectivity from the F-HSA–silica samples, measurements were carried out on the HSA/SM-30 system (48-Å radius nanoparticles) at the FIGARO reflectometer using subphases of buffered ACMW and buffered D$_2$O. SM-30 nanoparticles with a similar size to LS-30 were used because it had been shown since the LS-30 experiment above that SM-

30 silica sols were more stable. The use of contrast variation here allowed us to better define the scattering contributions from protein, nanoparticle and sub-phase at the air-water interface. ACMW and D_2O contrasts were used for each of four protein concentrations, ranging from 0.003 to 0.1 mg/mL while again keeping the concentration of silica nanoparticles constant at 0.6% v/v. Figures 9 (A) and

5 (B) show the RQ^4 reflectivity profiles and scattering length density profiles respectively, for both contrasts at the lowest F-HSA concentration of 0.003 mg/mL. Higher F-HSA concentration data (0.01, 0.03, and 0.1 mg/mL) have a similar appearance as expected from Figures 7 and 8. We conclude that a stable composite film of protein and silica is formed containing a 70-80 Å highly siliceous middle layer. The fitting parameters for the co-refinement are given in Table 7.

10
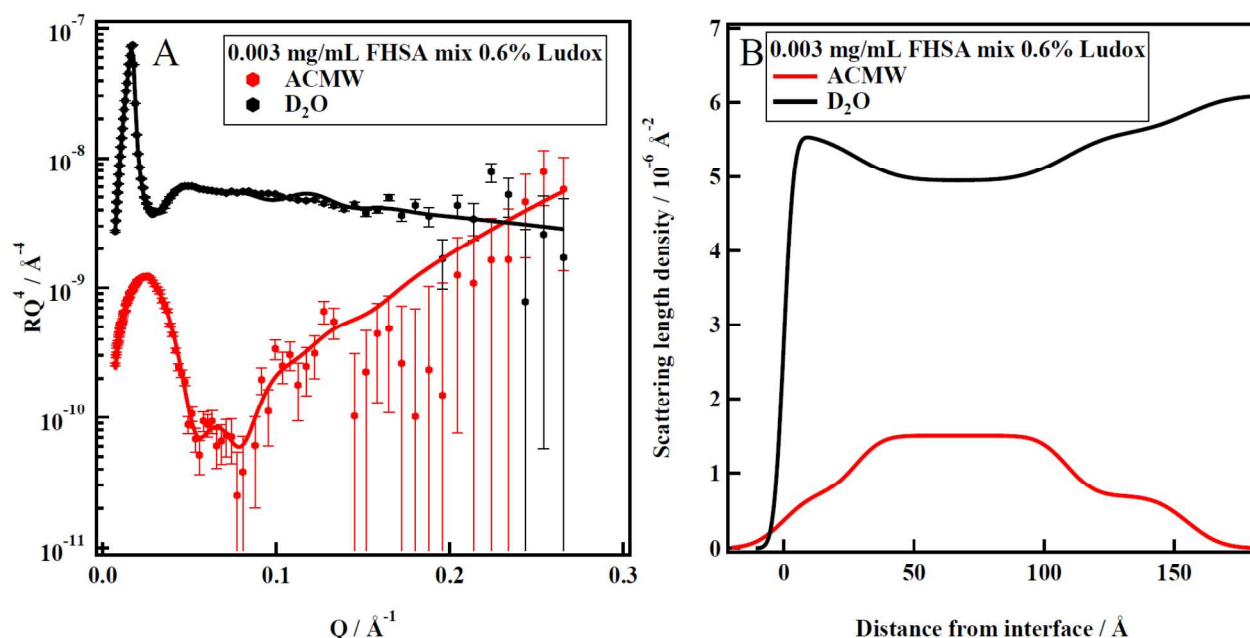
Fig. 9 (A) Fresnel-corrected reflectivity of ACMW (red) and D_2O (black) subphase contrasts for a 0.003 mg/mL F-HSA solution mixed with 0.6 v/v% silica nanoparticles. The SM-30 nanoparticles were used and the data were recorded on FIGARO. (B) Real space profiles obtained from model fitting of reflectivity data (solid lines) in (A).

15

The reflectivity profile for the ACMW contrast shows a distinct Kiessig fringe at low Q_z, similar to that seen in Figure 5 for the X-ray reflectivity of F-HSA/ SM-30. In ACMW, the protein-nanoparticle complex is in positive contrast at the interface and the subphase is matched to the scattering length of air. In contrast, with the D_2O subphase, the surface protein-nanoparticle complex is in negative

20 contrast ie. SLD-deficient compared to the subphase, hence, a minimum in the Kiessig fringe. The real space distribution (Figure 9 (B)) also shows this contrast difference. Convergent values of the layers' thicknesses allow satisfactory co-refinement of the two data sets with different contrasts[23].

Table 7 Co-refinement fitting parameters of the neutron reflectivity from ACMW and D$_2$O mixtures of F-HSA at 0.003 mg/mL with 0.6%v/v SM-30 silica

	ACMW	D$_2$O
τ_1/Å	27.8 (3.2)	27.8 (1.5)
ρ_1/10^{-6}Å^{-2}	0.7 (0.1)	5.6 (0.1)
τ_2/Å	81.1 (3.3)	81.1 (5.7)
ρ_2/10^{-6}Å^{-2}	1.5 (0.1)	4.9 (0.1)
τ_3/Å	46.3 (4.3)	46.3 (1.8)
ρ_3/10^{-6}Å^{-2}	0.7 (0.1)	5.6 (0.2)

Figure 10 (A) indicates that the thickness of the surface complex is nearly independent of the protein concentration for all three layers, so the minor fluctuations in layer thicknesses do not play a big role in the surface excess value changes. From that and focusing on the effect of increasing F-HSA concentration in the mixtures from 0.003 mg/mL to 0.03 mg/mL, Figure 10 (B) shows that the scattering length density of layer 2, in particular, decreased with increasing protein content. As (from the x-ray data) layer 2 has a lot of silica, the SLD decrease in this layer is indicative of some loss of that.

This is an important hint for understanding the DF-HSA data of Figures 7 and 8.
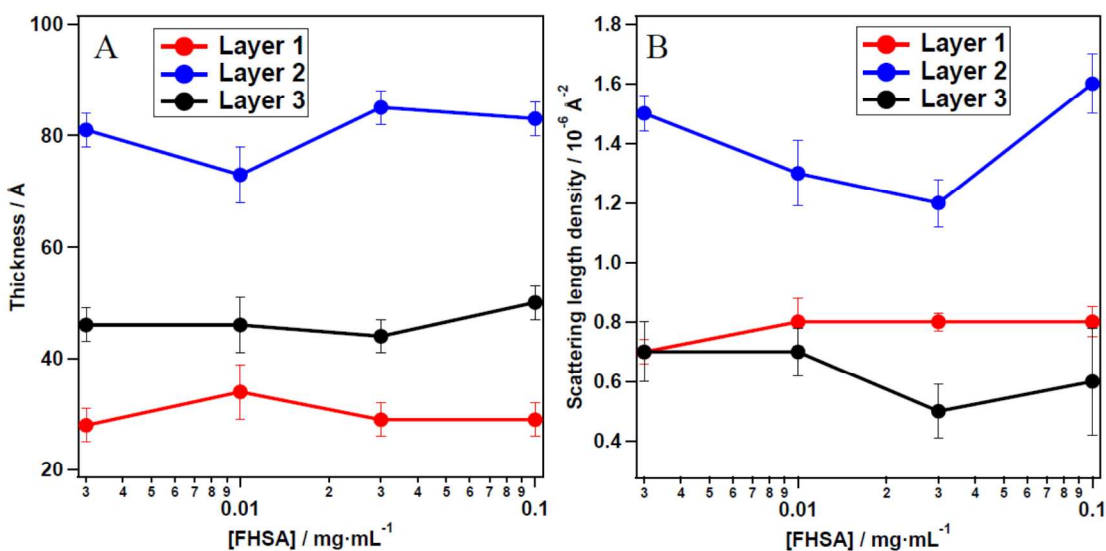
Fig. 10 (A) Thickness of individual layers making up the protein-nanoparticle complex at the air-water interface and (B) scattering length densities of layers as a function of F-HSA concentration.

3.7   Gel formation

Samples with the higher protein concentrations measured showed some opalescence in the DF-HSA samples after the experiments. The low concentration solutions did not. Observations over one week were made therefore, on solutions prepared in the same way. Gelling and sedimentation of the aggregates were observed, which did not occur in the diluted LS-30 or SM-30 mixtures at the same volume fraction without protein (See Supplementary information SI3 and SI4). As Figure 11 shows, this phase separation was more pronounced at lower concentrations of protein for the DF-HSA solutions than the F-HSA solutions.
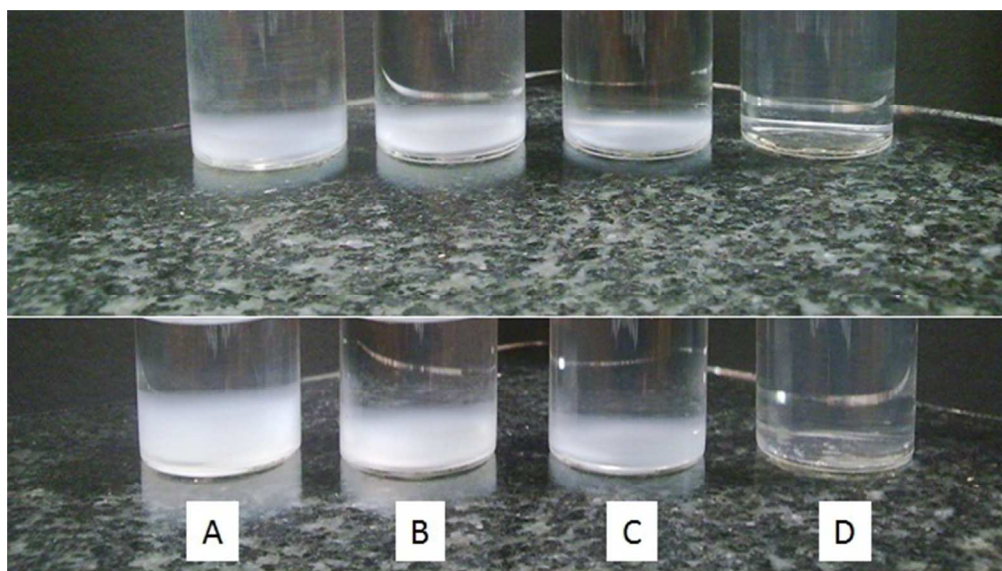
Fig. 11 Direct comparison of aggregation state between F-HSA (top) and DF-HSA (bottom) with silica nanoparticles left to stand over a period of a week. Decreasing protein concentrations from left to right in the order 2 > 1 > 0.1 > 0.01 mg/mL.

4   Discussion

4.1   HSA at the air-water interface - structure.

The structures of F-HSA and DF-HSA at the air-water interface depend on the protein concentration. At low concentrations (0.1 mg/mL) the neutron scattering length density and electron density of F-HSA have a film thickness of about 16 Å and an adsorbed amount of 1.4 mg/m^2. This thickness may correspond to an unfilled monolayer since the second layer does not appear until ca. 1 mg/mL, or could represent filling of the layer by the α helices of the molecule either through loss of tertiary structure at the interface as for myoglobin[21]or from the protein flexibility at low coverage. For concentrations above 1 mg/mL, the two layer fit gave a total thickness of about 45Å – the approximate size of packed undenatured molecules – possibly tilted. In the "train and loop" hypothesis (below) this would correspond to more loops pushed below the interface

The idea of partial filling of the surface layer by α-helices agrees with the chemically intuitive "train-and-loop" structure proposed by Graham and Phillips[20] in their extensive Langmuir trough study of the air water interface of HSA solutions. The high α-helical content (~60%) of HSA and the somewhat larger SLD of the low concentration layer in DF-HSA (less resistance to unfolding because of the fatty acid ligand) all point to this. In this hypothesis, the α-helices would form the highly packed "train" and the diffuse layer consists of "loops" composed of connecting segments between α-helices which protrude into the bulk subphase.

To test the "train and loop" hypothesis we calculated the relative electron density of the diffuse bottom layer to the dense top layer compared to the relative electron density of non-helical motifs from the crystal structure. Choice of different minimum lengths of amino acid residues allows the amount of non-helical parts excluded from the top dense layer to be tested against the reflectivity data. From Figure 4 and Table 3, the amount is 18% and 26% for the 1 and 10 mg/mL F-HSA adsorbed structures respectively.

This indicates that for the 1 mg/mL F-HSA solution structure at the interface, only non-helical fragments greater than 5 peptides long would extend into the subphase. However, in the adsorbed structure of 10 mg/mL F-HSA almost all non-helical components would be pushed into the bottom layer to satisfy the electron density found. This shows the extent of dense packing of helices in the

top layer.

Consideration of the hydropathy[24] of residues within the tail structure indicate that hydrophilic residues make up 68% of the "loops" compared to 54% in the helical part of the molecule. This is a 26% increase in the hydrophilic character for the "loops" compared to the helices in the top layer. The net charge of the residues making up the "loops" were also highly negatively charged. The combination of the increased hydrophilic character and highly charged "loops" at pH 7 makes them more susceptible to be in contact with the bulk subphase. The results are summarized in Table 8.

Table 8 Percentages of relative electron density contained within different minimum lengths of the "loops" of HSA calculated from the crystal structure and experimental results from Table 3.

	All non-helix	≥ 4 peptides	≥ 5 peptides	≥ 6 peptides
Calculated percentage (%)	27	24	21	13
Experimental percentage (%)	26 (10 mg/mL)	-	18 (1 mg/mL)	-
Percentage hydrophilic residues (%)	68	68	68	72
Net charge at pH 7	-10	-12	-13	-12

4.2   HSA at the air-water interface - Surface Excess.
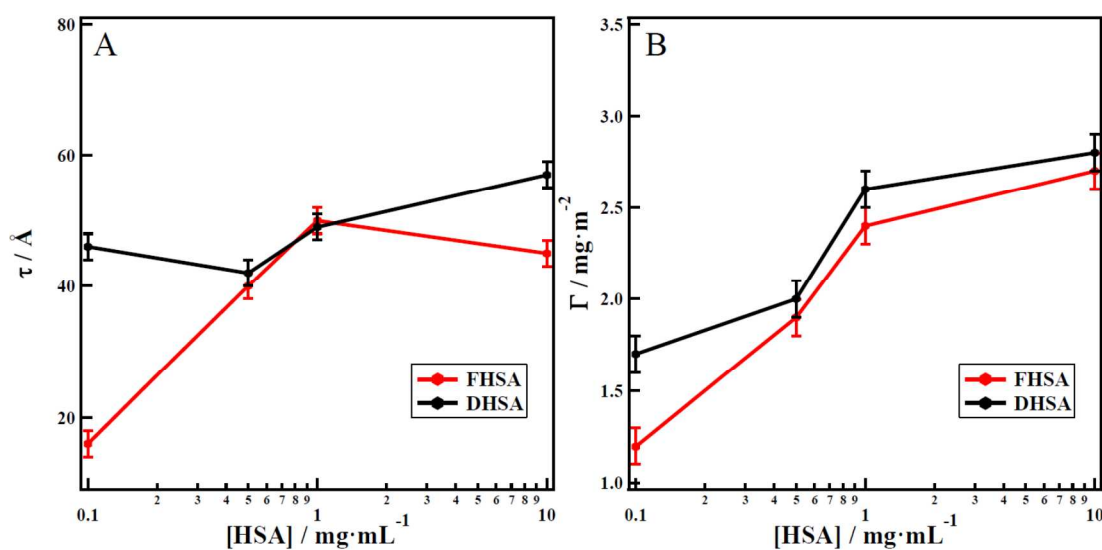
Fig. 12   Comparison of the total thickness (graph A) and surface excess (graph B) at the air-water interface as a function of protein concentration. F-HSA is shown in red and DF-HSA is black.

The surface activity of the two proteins as a function of solution concentration over three decades is an important datum for comparison with the outcomes of their mixtures with silica. Figure 12 and also, using neutron reflectivity, (Supplementary data Figure SI5) show that surface activities at all protein concentrations of DFHSA and FHSA are about the same. DFHSA is always slightly higher and the high layer thickness at 0.1 mg/mL also points to this difference in activity. Here, there is approximately 40% more DF-HSA adsorbed at the air-water interface compared to F-HSA.

4.3   Composition of the F-HSA and DF-HSA- Silica Interfacial Films.

The formation of films between human serum albumin and both LS-30 and SM-30 silica reveals differences in the surface interactions between the two protein nanoparticle forms. Because the results for DF-HSA showed a strong concentration dependence, we focus chiefly on the situation for the fatted protein because it is the natural form and also the films are robust and insensitive to the particle size.

The overall surface excess for F-HSA and DF-HSA-LS-30 silica (radius 42Å) is roughly proportional to the integral under the scattering intensity vs. depth profiles of Figure 8. For F-HSA this is constant over the wide concentration range of the PLATYPUS experiments. For DF-HSA it is lower than that for F-HSA at the lowest concentration, rises to about the same amount at 0.1 mg/ml protein and then drops to about half of this even though the depth distribution of DF-HSA is more extensive. The two proteins are interacting differently with the silica.

For the F-HSA/SM-30 silica (radius 48 Å) system, e.g. Figure 9B, the result is in qualitative agreement with that for F-HSA–LS-30. In this case the scattering length density profiles were derived by co-refinement of FIGARO data in ACMW and D_2O, and the surface excess of each component is shown in Figure 13. The relative amounts of each component in the film vary significantly with protein concentration between 0.003, 0.01, 0.03 and 0.1 mg/mL.
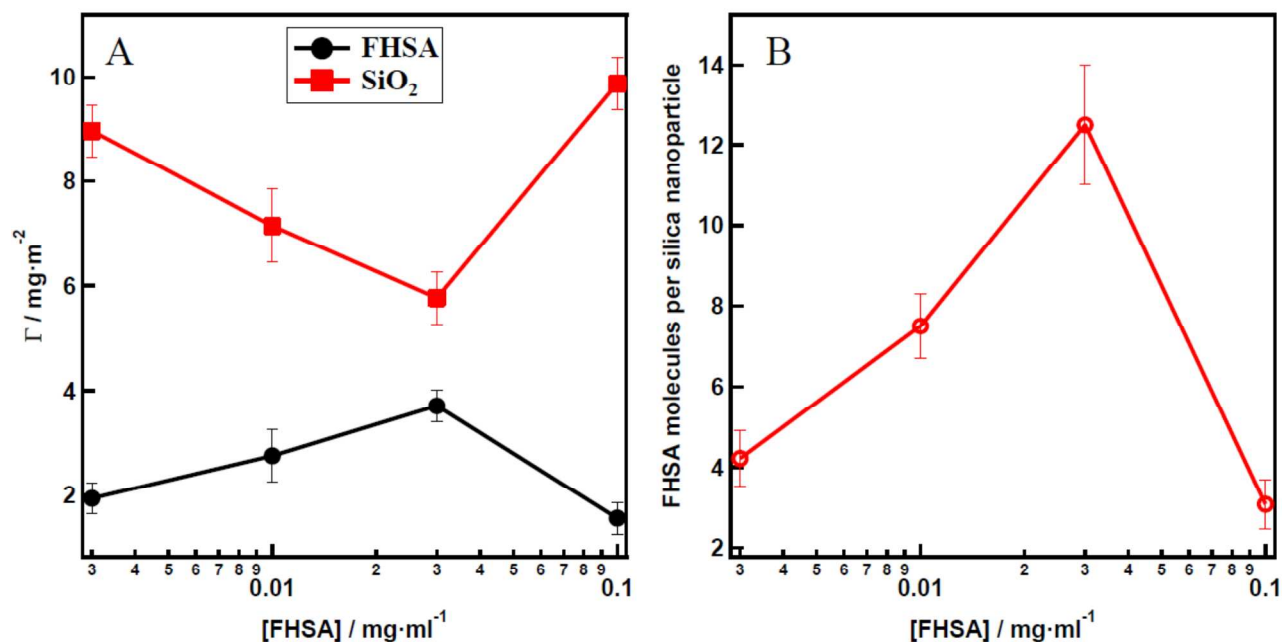
Fig. 13 (A) Surface excess of silica nanoparticles (red) and F-HSA (black) adsorbed at the air-water interface from F-HSA-SM-30 measurements at FIGARO. (B) Ratio of F-HSA molecules per nanoparticle at the air-water interface.

For the DF-HSA and F-HSA-LS-30 systems (PLATYPUS) another way of seeing the qualitative changes at high protein concentration is through the protein/silica nanoparticle ratio, Ψ , in the film (Figure 14). This is based on the surface excesses in Tables 9 and 10 and Equation 7. At protein concentrations greater than 1 mg/mL, the DF-HSA to SiO_2 content exceeds by a factor of 2-3 that observed for F-HSA indicating silica loss from the surface.
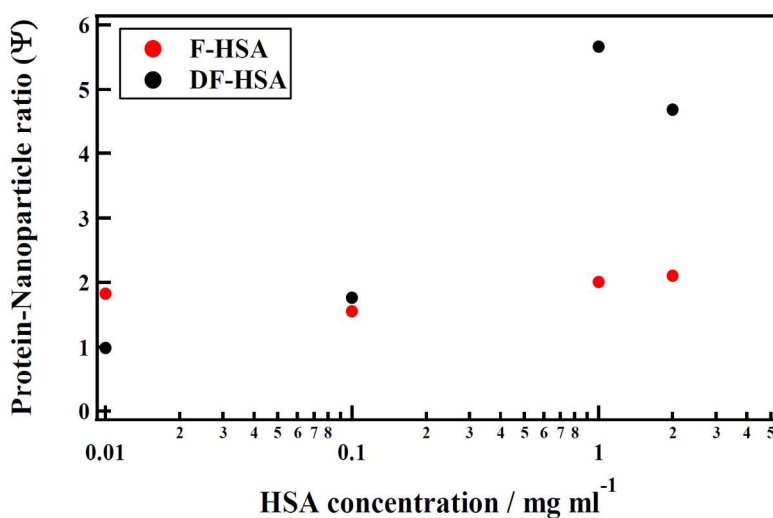
Fig. 14 Plot of protein to nanoparticle ratio (Ψ) as a function of HSA concentration within the adsorbed layer at the air-water interface from DF-HSA and F-HSA-LS-30 measurements at PLATYPUS.

Table 9 Surface excess in mg/m^2 of *protein* in the adsorbed interfacial layer.

Protein concentration (mg/mL)	F-HSA	DF-HSA
0.01	2.0	1.0
0.1	1.7	2.0
1.0	2.1	1.9
2.0	2.2	2.5

Table 10 Surface excess in mg/m^2 of *silica* in the adsorbed interfacial layer.

Protein concentration (mg/mL)	F-HSA	DF-HSA
0.01	5.7	5.3
0.1	5.9	6.1
1.0	5.5	1.8
2.0	5.5	2.9

A simple model for the composite film texture would be adsorption of un-deformed F-HSA molecules onto the silica nanoparticle with either the long or short axis of the molecule attached to the surface. For an 80-Å diameter silica nanoparticle, the available silica surface area of ~20000 Å^2 per particle would allow 3 or 9 protein molecules per nanoparticle respectively (assuming a protein surface area of ~5000 Å^2). This attachment would be the mechanism to bring the silica to the surface for the observed layer structure, presumably with excess protein attaching to the under-surface of the silica.

An alternative hypothesis is that protein adsorbs quickly to the interface and that silica particles attach themselves to it through hydrophilic interactions. This would imply that the surface structures quickly seen at all but the highest pH (Figures 5 and 6) and in the buffer solutions (Figures 7 and 8) quickly incorporate silica and a sub-layer of protein at the interface. The concentration-dependence of the structure formed for the DF-HSA system may be a clue to the different stability of this complex.

Other factors could affect this stability such as the number and rate of adsorption of pre-formed protein-silica complexes from solution compared to desorption of first formed silica-protein composites from the interface. Depletion resulting from gelation and sedimentation of aggregates under gravity, as has been shown recently for a synthetic polyelectrolyte/surfactant mixture,[25,26] may well be relevant for samples with high protein concentrations and particularly for DF-HSA as

suggested by the visual evidence in Figure 11). At present, however, we know little about the complexes in solution, their stability and their aggregation once formed in the solution phase and their surface activity if preformed.

4.5   Molecular basis of F-HSA and DF-HSA differences

The difference in the interaction behavior of F-HSA and DF-HSA with SiO_2 nanoparticles as observed by neutron reflectometry at the air-water interface, CD measurements and aggregation in the bulk phase, may be attributed to a combination of conformational stabilisation, different electrostatics and specific protein- peptide binding.

4.5.1   Stabilization of HSA conformation by fatty acids. UV circular dichroism (CD)[27], shows that silica nanoparticle mixtures with the proteins in buffer induces a smaller denaturing effect on the secondary structure of F-HSA than for DF-HSA. Fatty acid anchored in the hydrophobic high-affinity binding sites 4 and 5 confers structural stability to Domain III by the hydrocarbon tail of the FA stabilizing hydrophobic clefts in the binding sites[10]. This makes F-HSA more rigid than DF-HSA and we suppose this structure to be less able to adopt conformations which minimize the electrostatic energy in the presence of the silica. So a weaker interaction with the silica occurs.

4.5.2   Electrostatic interaction between HSA and nanoparticles. Although fatty acids reduce the net charge on HSA by binding to the positive residues (Curry et al[10]), the effect is weak, since even when seven fatty acids are bound, there is no significant effect on the distribution of positive charges. On the other hand the distribution of the charges on the protein is of significant interest[28].

The sensitivity to the buffer ionic strength of the adsorbed amount of silica to F-HSA shows the presence of an electrostatic component to the HSA-silica interaction. Between zero molar sodium chloride and 50 mM the scattering length density in the silica containg region of the film (25 Å to 80 Å) below the air-water interface, increases from 1.2 to 1.6 x 10^{-6} Å^{-2} [29]. At 200 mM this drops[23] to 1.5 x 10^{-6} Å^{-2} .

As the isoelectric points (IP) of F-HSA and DF-HSA are 4.7 and 5.8 respectively and that for silica is just above 2 (Table 1) all species are negatively charged in the descending order silica > F-HSA > DF-HSA. The silica nanoparticle surface is negatively charged, as indicated by the large zeta potential[29,30] of -45 mV at pH 7 (charge per particle of -13). Thus from the IP, the overall F-HSA–silica repulsion is greater for F-HSA than for DF-HSA. With the assumption that the attractive interactions from hydrophobic interactions and specific peptide-silica binding are the same for each protein, F-HSA binding to silica is the weaker.

Other attractive electrostatic interactions are those between peptides and silica discussed by Livage[31] for peptide- silica mixtures. There the silica is first adsorbed onto peptides containing an NH_3^+ group to form aggregates that then flocculate in the presence of additional peptides. As HSA has 59 Lysine molecules with a charge of +1 each at pH = 7 the same type of electrostatic forces may contribute stability to the complexes.

That these efects are quite general is shown by Tenzer et al[32]. They examined a wide range of nanoparticle sizes and proteins forming "coronas" using electron microscopy and chromatographic methods. Our data here agree with theirs in that, despite the strong negative charges on the species, extensive interaction between protein and silica occurs quickly. Furthermore their zeta potential measurements (eg -12.2mV) show that negative charge persists on the whole complex implying a distributed adhesion of the protein and particle.

4.6   Hydrophobic interactions and gelling

The extent of hydrophobic contributions to the attractive forces can be gauged from the neutron reflectivity experiments of Foster et al[33] where no adsorption of F-HSA occurred with a water-wettable SiO_x surface. For a hydrophobic surface (NH_3^+ terminated self-assembled silane monolayers), however, there was strong adsorption. Considering a silica nanoparticle of radius 42Å and charge -13 the surface charge density is low, so the exposure of hydrophobic silica is large and a hydrophobic contribution to the negative enthalpy of adsorption is plausible.

The tendency of HSA to aggregate – though highly charged at pH 7 has been shown by light scattering experiments[34] and this is faster for DF-HSA at 25C than for F-HSA. We relate this again to the effect of fatty acid on the protein reactivity. Domain III contains two high-affinity fatty binding sites[13] and is the most important domain in albumin for their binding. There is thus an asymmetric distribution of fatty acid in the F-HSA structure which could limit the accessibility of nanoparticle-protein binding to Domains I and II.

4.6.1   Gelling

We attribute this again to the differences in the two protein molecules outlined above and that binding of SiO_2 to F-HSA in Domain I reduces the extent of aggregation caused by formation of

intermolecular disulfide bonds through Cys_{34}. This can been seen as a "self-protection" mechanism of F-HSA in its interaction with the nanoparticles. In DF-HSA, all three domains are equally available for interaction with the silica nanoparticles, the occupancy of Domain I by the SiO_2 particles is lower than F-HSA, allowing DF-HSA to be more susceptible for disulfide bonding and hence more precipitation in the bulk.

5   Conclusions

Although the rate of formation of silica-containing protein films at the air-water interface of F-HSA and DF-HSA is fast for both molecules with SM-30 silica nanoparticles as the substrate, the structural outcomes from the two variants of the human serum albumin are significantly different. The F-HSA films are independent of protein concentration but those for the defatted form are strongly dependent on protein concentration. Both proteins and silica have high negative charge at the physiological pH used. The differences in behaviour are attributed to stabilising effects on the protein conformation of the fatty acid ligand – for F-HSA, electrostatic effects – and also to a related tendency for aggregation in DF-HSA. The same difference in behaviour leads to faster protein-induced gelling for the DF-HSA-silica mixtures and we conclude that protein-silica complexes must be formed in solution through hydrophobic and specific forces between the two components leading to either long-term or transient surface activity for the silica but eventual gel precipitation.

6   Acknowledgements

7   Notes and references

[a] *Research School of Chemistry, Australian National University, Canberra, ACT 0200, Australia. Fax: +61 2 6125 4903; Tel: +61 2 6125 3578; E-mail: jww@rsc.anu.edu.au*

[b] *Current address:*

[c] *Bragg Institute, Australian Nuclear Science and Technology Organization, Menai, NSW 2234, Australia*

[d]*Institut Laue Langevin, Grenoble, France*

1. I. Lynch, T. Cedervall, M. Lundqvist, C. Cabaleiro-Lago, S. Linse and K. A. Dawson, *Adv. Colloid Interface Sci.*, 2007, **134**, 167-174.

2. M. P. Monopoli, C. Arberg, A. Salvati and K. A. Dawson, *Nat. Nanotechnol.*, 2012, **207**, 779-786.

3. L. C. J. Thomassen, A. Aerts, V. Rabolli, D. Lison, L. Gonzalez, M. Kirsch-Volders, D. Napierska, P. H. Hoet, C. E. A. Kirschhock and J. A. Martens, *Langmuir*, 2010, **26 (1)**, 328–335.

4. J. C. Ang, J. M. Lin, P. N. Yaron and J. W. White, *Soft Matter*, 2010, **6**, 383-390.

5. J. Penfold, *Current Opinion in Colloid & Interface Science*, 2002, **7**, 139-147.

6. C. Leggio, L. Galantini and N. V. Pavel, *Phys. Chem. Chem. Phys.*, 2008, **10**, 6741-6750.

7. T. J. Peters, All About Albumin: Biochemistry, Genetics and Medical Applications, San Diego Academic Press, 1996.

8. J. Ghuman, P. A. Zunszain, I. Petitpas, A. A. Bhattacharya, M. Otagiri and S. Curry, *J. Mol. Biol.*, 2005, **353**, 38-52.

9. D. C. Carter and J. X. Ho, *Adv. Protein Chem.*, 1994, **45**, 153-203.

10. A. A. Bhattacharya, T. Grune and S. Curry, *J. Mol. Biol.*, 2000, **303**, 721-732.

11. L. G. Longsworth and C. F. Jacobsen, *J. Phys. Colloid Chem.*, 1949, **53**, 126-135.

12. E. Gianazza, A. Frigerio, S. Astruatestori and P. G. Righetti, *Electrophoresis*, 1984, **5**, 310-312

13. J. R. Simard, P. A. Zunszain, C. E. Ha, J. S. Yang, N. V. Bhagavan, I. Petitpas, S. Curry and J. A. Hamilton, *Proc. Nat. Acad. Sci. USA*, 2005, **102**, 17958-17963.

14. S. Curry, Drug Metab. Pharmokinet. 2009, **24**,342-357

15. C. Leggio, L. Galantini, P. V. Konarev and N. V. Pavel, *J. Phys. Chem. B*, 2009, **113**, 12590-12602.

16. A. S. Brown, S. A. Holt, P. M. Saville and J. W. White, *Aust. J. Phys.*, 1997, **50**, 391-405.

17. M. James, A. Nelson, A. Brule and J. C. Schulz, *J. Neutron Research*, 2006, **14**, 91–108.

18. R. A. Campbell, H. P. Wacklin, I. Sutton, R. Cubitt and G. Fragneto. *European Physical Journal Plus* 2011, **126**, 107."

19. A. Nelson, *J. Appl. Crystallography*, 2006, **39**, 273-276.

20. D. E. Graham and M. C. Phillips, *J. Colloid Interface Science*, 1979, **70**, 403-414.

21. S. A. Holt, D. J. McGillivray, S. Poon and J. W. White, *J. Phys. Chem. B*, 2000, **104**, 7431-7438.

22. J. R. Lu, T. J. Su and J. Penfold, *Langmuir*, 1999, **15**, 6975-6983.

23. J. C. Ang PhB Thesis Australian National University 2013

24. J. Kyte and R. F. Doolittle, *J. Mol. Biol.*, 1982, **157**, 105-132.

25. R.A.Campbell, M. Y. Arteta, A. Angus-Smyth, T. Nylander, I.Varga, *J. Phys. Chem. B*, 2012, **116**, 7981-7990.

26. R.A.Campbell, M. Y. Arteta, A. Angus-Smyth, T. Nylander, I.Varga, *J. Phys. Chem. B*, `2011*, **115***, 15202-15213

27. J. C. Ang, J. M. Lin, P. Yaron and J. W. White submitted *Biochem. Biophys. Acta*

28. H. Bysell, P. Hansson and M. Malmsten, *J. Phys. Chem. B*, 2010, **114**, 7207-7215.

29. D. Lee, Z. Gemici, M. F. Rubner and R. E. Cohen, *Langmuir*, 2007, **23**, 8833-8837.

30. B. Bharti, J. Meissner and G. H. Findenegg, *Langmuir*, 2011, **27**, 9823-9833.

31. T. Coradin, O. Durupthy and J. Livage, *Langmuir*, 2002, **18**, 2331-2336.

32. S. Tenzer, D. Docter, S. Rosfa, A. Wlodarski, J. Kuharev, A. Rekik, S. K. Knauer, C. Bantz, T. Nawroth, C. Bier, J. Sirirattanapan, W. Mann, L. Treuel, R. Zellner, M. Maskos, H. Schild and R. H. Stauber, *ACSNANO*, 2011, **5,** 7155-7167.

33. A.Liebmann-Vinson, L. M. Lander, M.D. Foster, W. J. Brittain, E. A. Vogler, C. F. Majkrzak and S.Satija, *Langmuir*, 1996**, 12***, 2256-2262.

34. D. Hess and J. W. White (in preparation).

Colour Graphic PCCP 17-2-14